

New operando method for quantifying the relative half-cycle rates of the NO SCR redox cycle over Cu-exchanged zeolites

W.P. Partridge^{a,*}, S.Y. Joshi^b, J.A. Pihl^a, N.W. Currier^b

^a Oak Ridge National Laboratory, 2360 Cleghorn Blvd., Knoxville, TN, 37932, United States

^b Cummins Inc, 1900 McKinley Ave, Columbus, IN, 47201, United States



ARTICLE INFO

Keywords:

NH₃SCR
Cu redox half cycles
Kinetic model
Operando SpaciMS

ABSTRACT

An operando experimental method for monitoring relative variations in half-cycle rates of the Cu redox-cycle model of selective-catalytic-reduction (SCR) is demonstrated, along with a kinetic model for predicting the same. Conversion inflections (CI) can occur at SCR onset within Cu/SCR catalysts; transient CI involves initial conversion growth to an intermediate value greater than exists at steady state (SS) before degrading to the SS value. While similar CI has been reported for Fe/SCR catalysts as being due to NH₃ inhibition, Cu/SCR CI is inconsistent with a similar origin. Rather, Cu/SCR CI is due to imbalances in the redox-half-cycle rates, and will occur when reduction is faster than oxidation. The temporal CI shape varies with the redox-cycle kinetic parameters and model formulation, and can be used to study the same. We demonstrate the first measurements of dynamic half-cycle rate balancing at SCR onset, use CI and onset transients to study variations in half-cycle rates under Standard, Fast and NO₂ SCR, and present the first redox-cycle model showing CI. The new operando method and model provides a basis for better understanding the SCR redox process, and determining the individual half-cycles kinetic model formulation and parameters.

1. Introduction

Conversion inflections have been measured at SCR onset within model Cu-BETA and commercial Cu/CHA catalysts [1,2], and are characterized by fast, step-like conversion growth to an intermediate level greater than the SS conversion, and slow conversion degradation to that SS level. To convey some general aspects of CI nature, Fig. 1 shows SCR-onset N₂ transients for a commercial Cu/CHA SCR catalyst over a range of conditions. At 400 °C, CI is observed for Standard SCR, but not Fast SCR which has a step-like onset transient. At 500 °C, CI is observed for both Standard and Fast SCR; the Standard-SCR CI appears faster and more distinct compared to 400 °C, and while CI is observed for Fast SCR at 500 °C it is significantly less distinct than for 500 °C Standard SCR. Similar measurements at 200 and 600 °C, confirm that CI becomes progressively more pronounced (faster transient) with increasing temperature over this range. Spatiotemporally distributed CI transients are typically observed only within the catalyst, are most pronounced at the catalyst front where NH₃ and NO_x concentrations are high, and become progressively less distinct through the SCR zone (spatial range over which NO_x and NH₃ are consumed); e.g., see Fig. 2. The spatiotemporal data of Fig. 2 covers a range of space velocities and feed concentrations, and provides insights regarding the impact of such

variations on CI transients; i.e., each fractional length has a different SV (e.g., 160 k hr⁻¹ at 1/4 L) and inlet concentration (each successive catalyst section has a progressively lower feed concentration). Because Cu/SCR CI has only been observed within those catalysts and not in the effluent, it has not been broadly reported or recognized to exist. When CI exists, anything (e.g., ageing, SV) that cause high NH₃ and NO_x concentrations to exist deeper into the catalyst will result in CI existing proportionally deeper into the catalyst [2]. Transient CI occurs only at SCR onset, and not at SCR termination. In general, CI increases with temperature, is most apparent with Standard SCR, and only with Fast SCR at higher temperatures.

Conversion inflections have been reported in the effluent of Fe/SCR catalysts and attributed to transient NH₃-coverage buildup and depletion through a threshold level corresponding to the onset of NH₃ inhibition at SCR onset and termination [3, Appendix A]. Such NH₃-inhibition-induced CI occurs at both SCR onset and termination, and should be more pronounced at conditions with higher NH₃ storage capacity; i.e., greater at lower temperature, and less pronounced at higher temperatures where NH₃ capacity is lower. The CI observed for Cu/SCR catalysts is inconsistent with these features of inhibition-induced CI, which suggests a different origin. Moreover, the Cu/SCR CI nature is not captured by incorporating an inhibition term into a kinetic

* Corresponding author.

E-mail address: partridgewp@ornl.gov (W.P. Partridge).

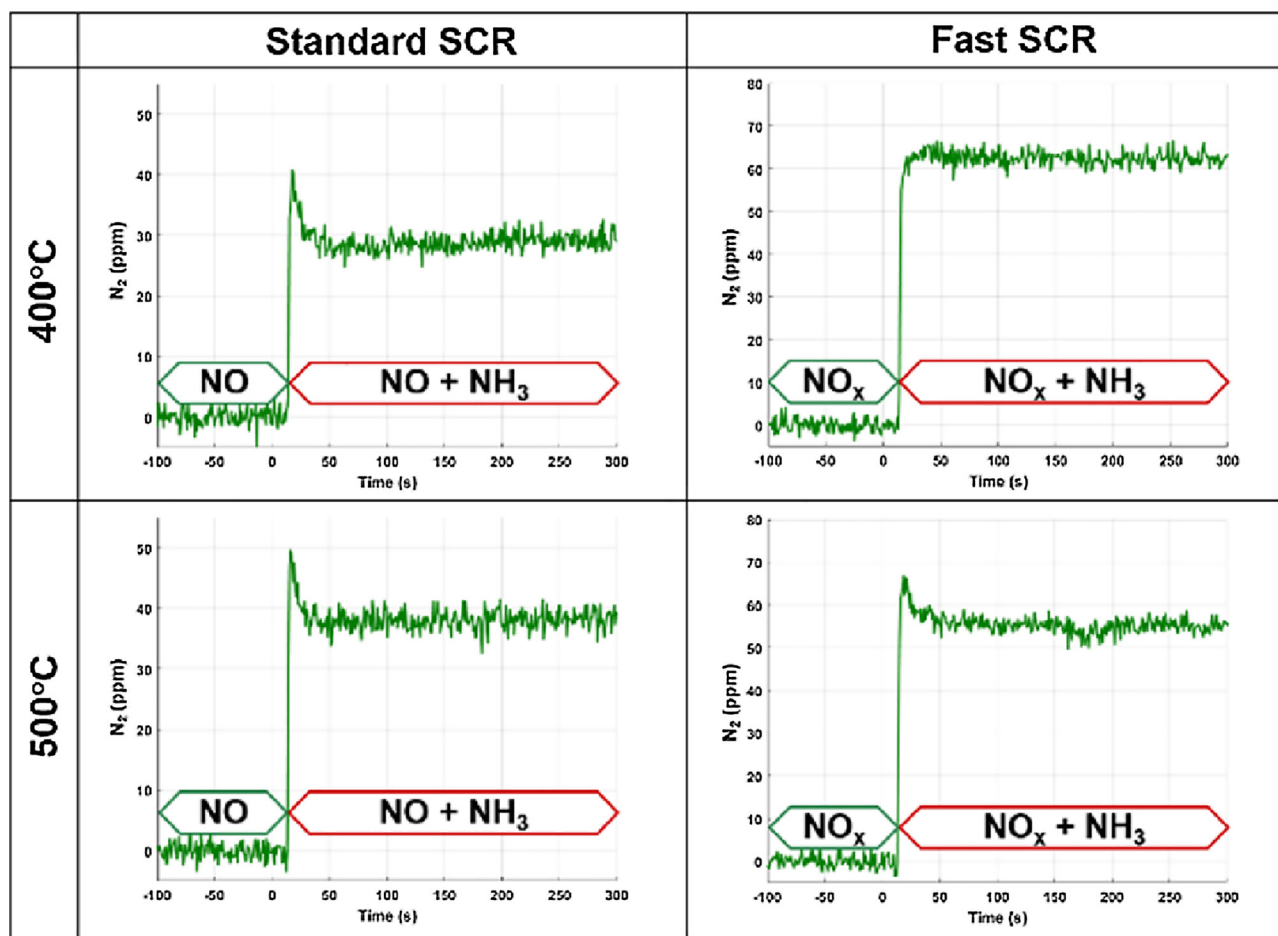


Fig. 1. N_2 transients associated with SCR-onset at 400 (top) and 500°C (bottom), and under Standard (left) and Fast (right) SCR conditions. Field aged commercial Cu/CHA, 300 ppm NO_x + 300 ppm NH_3 + 10% O_2 + 5% H_2O + Ar balance, 400cpsi, 40 k hr^{-1} SV, 1/8 length from catalyst inlet.

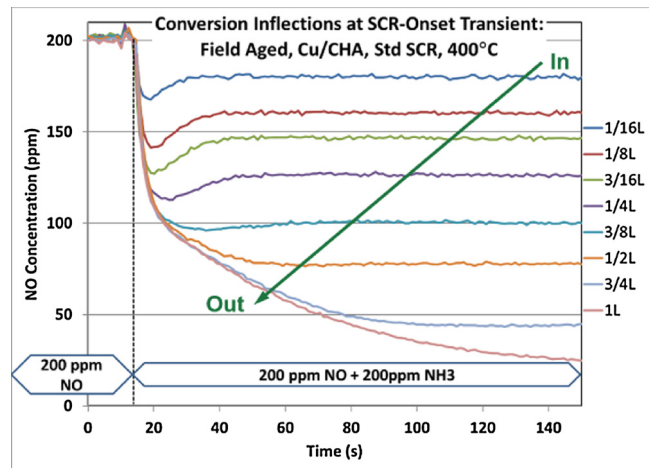


Fig. 2. Spatiotemporally resolved SCR-onset transients throughout a field aged, commercial, 400cpsi, honeycomb-monolith-supported Cu/CHA catalyst, where L is the overall catalyst length; [2] 200 ppm NO + 200 ppm NH_3 + 10% O_2 + 5% H_2O + Ar balance, 400°C, 400cpsi, 40 k hr^{-1} SV. Measurements via direct-sampling SpaciMS using 200 μm OD capillaries with ca. 10 $\mu\text{L}/\text{min}$ sampling rate for intra-catalyst spatiotemporally resolved concentration measurement [12–15]. Conversion inflections are most distinct at the catalyst inlet where NO and NH_3 concentrations are greatest, CI progressively degrades along the catalyst axis as conversion progresses, and is not apparent in the catalyst back half and effluent.

model.

We demonstrate through experimental measurement and modeling that Cu/SCR CI is due to imbalances in the half-cycle rates of a cyclic Cu reduction and oxidation (redox) process. A kinetic model is presented and exercised to demonstrate the dependence of the CI nature on various half-cycle kinetic parameters and application conditions (concentrations and temperature); the model demonstrates the ability to model transient Cu/SCR CI via the two half cycles. The measurements and models are the first we know of to resolve dynamic balancing of the half-cycle rates at SCR onset, and to demonstrate transient CI associated with the individual and combined half cycles, respectively. The new operando experimental method and model provides a basis for better understanding the SCR redox process, and determining the individual half-cycles kinetic model formulation and parameters.

2. Conceptual model of Cu/SCR-Onset CI

Several groups have cast the Cu/SCR process in terms of cyclic Cu reduction and reoxidation (redox) [4–13]. The SCR redox cycle can be viewed as two half cycles; the reduction half cycle (RHC) and the oxidation half cycle (OHC) as shown in Fig. 3a. In the RHC, oxidized Cu (Cu^{II}) is converted to reduced Cu^I in a reaction consuming NH_3 and NO and producing N_2 . In the OHC, Cu^I is reoxidized to Cu^{II} , completing the cycle. The RHC and OHC rates are proportional to Cu^{II} and Cu^I concentrations, respectively, and thus will vary as the partitioning of the Cu inventory between the two states varies; OHC can proceed via O_2 and NO_2 pathways, with NO_2 being preferable as it is first order in Cu^I and can activate isolated Cu sites [12].

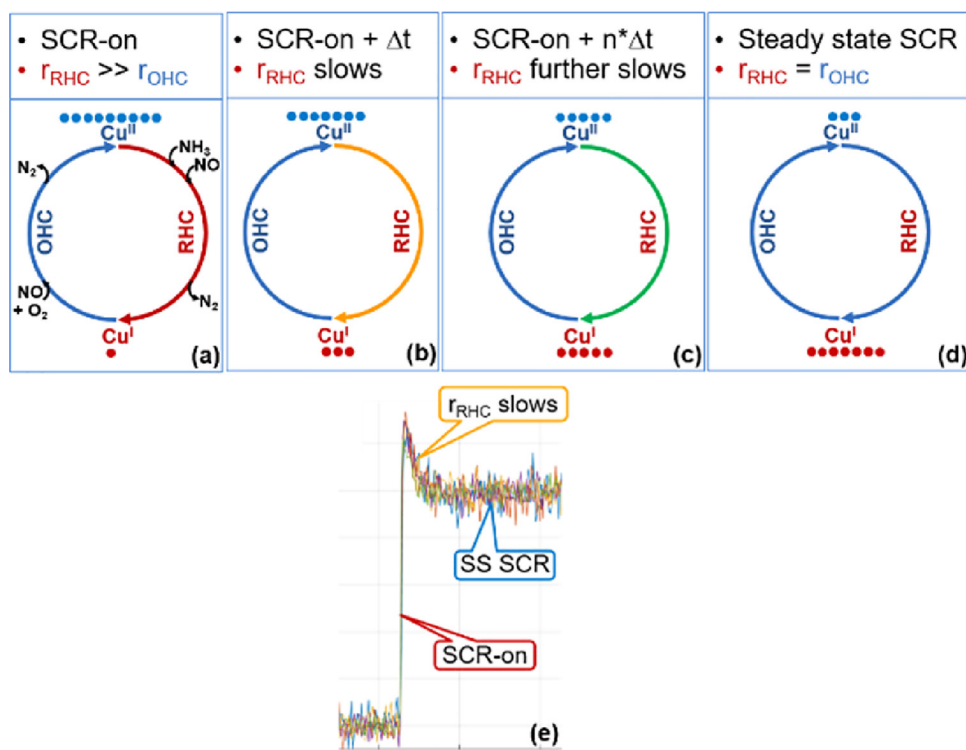


Fig. 3. (a) Schematic of SCR Cu redox cycle, composed of RHC and OHC half cycles. (a-d) Four-panel diagram highlighting variations in RHC and OHC rates, and partitioning of the Cu inventory between Cu^{II} and Cu^I through the SCR-onset transient. (e) An SCR-onset CI transient labelled corresponding to a-d.

Fig. 3 demonstrates how RHC and OHC rate imbalances lead to SCR-onset CI, and specifically how CI is indicative of the native RHC rate (r_{RHC}) being faster than the OHC rate (r_{OHC}). Before SCR onset, in the absence of NH₃, the Cu inventory is significantly biased to Cu^{II}; this is visually represented in Fig. 3a, by the 9 blue dots depicting Cu^{II} and single red dot depicting Cu^I. When CI occurs at SCR onset, r_{RHC} is much faster than r_{OHC} , resulting in very fast step-like conversion increase at the transient onset; labeled on the Fig. 3e CI profile. However, as RHC is depleting Cu^{II} faster than it is being repopulated by OHC, the Cu^{II} concentration decreases, and RHC slows accordingly; this progressive Cu^{II} depletion and corresponding RHC slowing is highlighted by Fig. 3b–c and continues until an SS $r_{RHC}=r_{OHC}$ balance is reached (see Fig. 6d). Conversion degrades as RHC slows resulting in a CI as labeled in Fig. 3e; this is most apparent if only RHC-attributable N₂ is considered, but the more complicated and realistic situation of N₂ generation from both half cycles is addressed via the following modeling discussion. At SS, RHC has slowed to match the OHC rate, and the Cu-inventory partitioning has redistributed accordingly. The appearance of a CI further indicates that the Cu-partitioning redistribution process is slower than the initial RHC rate, as is natural for such codependent rates; i.e., where the two rates influence each other via their influence on Cu-redox partitioning. The half-cycle kinetic parameters influence the specific transient CI shape; and thus, the CI temporal shape can provide information regarding the RHC and OHC kinetic parameters. To summarize, CI occurs when r_{RHC} is faster than r_{OHC} , and is created by progressive RHC slowing due to Cu^{II} depletion until it matches r_{OHC} at SS. Correspondingly, anything that speeds r_{OHC} relative to r_{RHC} will mitigate CI; similarly, CI will be more pronounced as the ratio of the half-cycle rates (r -ratio = r_{RHC}/r_{OHC}) increases. Moreover, as demonstrated in Section 3, while CI will occur at r -ratios greater than unity, it will be most apparent and distinct at higher absolute rates even for a fixed r -ratio. Furthermore, CI due to half-cycle rate imbalances will only occur at SCR onset and not termination; at termination, the Cu^{II}-biased partitioning of the natural oxidized state will be reestablished at the slower OHC rate.

Others have described non-redox models for Fast and NO₂ SCR, based on reduction and decomposition of nitrates [14]. The observation of Fast-SCR CI at higher temperatures, suggests that even if the nitrate route is predominant at low-mid temperatures, the redox cycle (or some other CI-producing phenomena) is becoming significant at higher temperature. The operando CI methodology and models described here provide a basis for studying these complex issues.

3. Kinetic models of the Cu/SCR redox cycle

Two-step (RHC & OHC), kinetic models for Standard and Fast SCR were formulated and exercised to demonstrate how RHC-OHC rate imbalances create CI, and how the CI nature changes with environmental conditions, and model formulation and kinetic parameters. The RHC rate was modeled as first order in Cu^{II} and NO (Eqs. (1) & (2)), and is common to both Standard and Fast SCR. Ammonia coverage, θ_{NH_3} , is a very weak function of gaseous NH₃ concentration over a wide range of temperatures including the range studied here, and thus RHC is considered zeroth order in θ_{NH_3} . The cited literature indicates much greater uncertainty in the OHC half-cycle reaction network; e.g., the Standard-SCR OHC reaction can be formulated with or without reactant NO, which will impact the CI shape, but not its existence. The Standard SCR OHC was formulated to function via a Cu dimer, (NH₃)₂Cu^{II}-O₂-Cu^{II}(NH₃)₂, and incorporate NO in the second part of the OHC reaction to be consistent with recent literature [12]; the rate is first order in O₂ and NO, and second order in Cu^I due to the intermediate Cu dimer (Eq. (4)). The Cu-dimer intermediate of Standard SCR OHC, limits the active Cu sites via proximity and pairing requirements [12]. In contrast, NO₂ can directly oxidize the individual NH₃-solvate Cu^I sites, and thus Fast SCR engages a greater fraction of the total Cu sites [12]. Correspondingly, the Fast SCR OHC was formulated as in Eqs. (6) and (7) with a rate first order in Cu^I and NO₂. Eqs. (5) and (8) show that the net of these half-cycle formulations are consistent with the Standard and Fast SCR reactions, respectively [14]. The detailed microkinetic steps of the Cu-SCR redox cycle are the focus of and can be studied in the cited

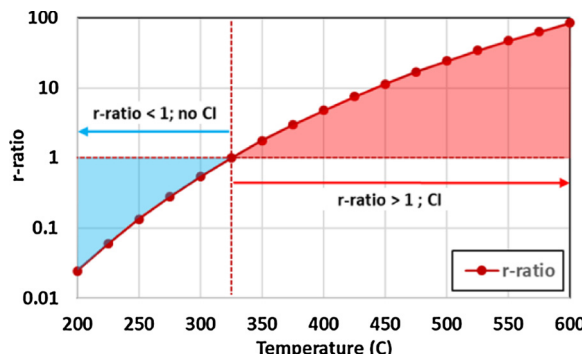


Fig. 4. Results from a two-step kinetic model of the Standard Cu/SCR redox cycle demonstrating how RHC-OHC rate imbalances produce CI. Temperature variation in the r-ratio. Activation energies of 140 and 70 kJ/mole were used for RHC and OHC, respectively, in this example.

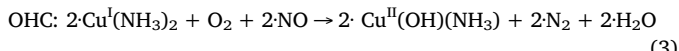
literature [4–13], and the formulation of Eqs. (1)–(8) is primarily based on the recent work of Paolucci et al. [4,11,12]. The model is sufficient to demonstrate how half-cycle rate imbalances induce CI, and the dependence of CI on half-cycle-reaction formulation and the kinetic parameters; and correspondingly, the ability of transient-response CI analysis to guide reaction formulation and determination of half-cycle kinetic parameters.

There are several considerations impacting the applicability of a kinetic SCR model across different catalyst and conditions. Because OHC occurs via different pathways for Standard and Fast SCR, it has been suggested that a mean-field model may not faithfully capture actual catalyst performance; [12] i.e., because the rates and number of Cu sites participating in the two SCR types differs. Certainly Eqs. (3)–(4) & (6)–(7) support this observation, and the perspective that while a model may apply to a given SCR type, there could be confusion with mixed or simultaneous Standard and Fast SCR. However, experiments have shown at NO_x stoichiometries where simultaneous Standard and Fast SCR is theoretically possible, that practically the two SCR types occur sequentially, [15] i.e., SCR proceeds solely via Fast SCR until NO_2 is depleted, followed by Standard SCR to completion. Thus, while these SCR-type-specific differences in OHC and corresponding model implications are important to recognize, it may be possible to use such “additional” knowledge to resolve the apparent model limitations. Another consideration is differing kinetics for 1 Al- vs 2 Al-coordinated Cu species [11], which could complicate application of a model in conditions of varying reaction partitioning between the various Cu coordinations. However, for a given catalyst (Si:Al ratio) this partitioning is expected to be fixed allowing applicability of a mean-field model; presumably a more complete model would incorporate dedicate half-cycle formulations for the individual coordinations, but each similar to that shown here. Thus, within an SCR type and a given catalyst, the model represented by Eqs. (1)–(8) is appropriate for the CI study presented here. While a detailed model will allow more comprehensive exploration of the CI phenomenon and is the focus of our ongoing work, the kinetic model presented here is sufficient for demonstration and identifying CI trends.

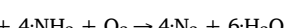
3.1. Standard SCR



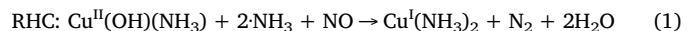
$$r_{\text{RHC}} = k_{\text{RHC}} \cdot [\text{Cu}^{\text{II}}] \cdot [\text{NO}] \cdot (\theta_{\text{NH}_3})^{-0} \cong k_{\text{RHC}} \cdot [\text{Cu}^{\text{II}}] \cdot [\text{NO}] \quad (2)$$



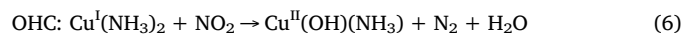
$$r_{\text{OHC,S}} = k_{\text{OHC,S}} \cdot [\text{Cu}^{\text{I}}]^2 \cdot [\text{O}_2] \cdot [\text{NO}] \quad (4)$$



3.2. Fast SCR



$$r_{\text{RHC}} = k_{\text{RHC}} \cdot [\text{Cu}^{\text{II}}] \cdot [\text{NO}] \cdot (\theta_{\text{NH}_3})^{-0} \cong k_{\text{RHC}} \cdot [\text{Cu}^{\text{II}}] \cdot [\text{NO}] \quad (2)$$



$$r_{\text{OHC,F}} = k_{\text{OHC,F}} \cdot [\text{Cu}^{\text{I}}] \cdot [\text{NO}_2] \quad (7)$$



3.3. Modeling results and discussion

While CI will occur for various model formulations and kinetic parameters, there is a unique formulation and parameter set appropriate for a given catalyst, and which will accurately describe the transient CI nature. In the in this section, the model is exercised to generally demonstrate how the transient CI nature varies with environmental-conditions and kinetic-parameter variations. Although results are shown for only one model formulation, CI occurs for various model formulations (e.g., OHC with and without NO participation), and the specific CI nature will change accordingly. Thus, detailed CI analysis can be used to guide determining the correct model formulation. The purpose is to demonstrate how transient-response CI analysis can be used to guide model formulation and kinetic-parameter determination.

Fig. 4 shows how the r-ratio varies with temperature; the RHC and OHC pre-exponential factors were adjusted to cause the r-ratio to equal unity at ca. 325 °C, corresponding to the experimentally observed CI onset. The r-ratio increases with temperature. CI occurs for r-ratios greater than unity, and will become increasingly distinct for greater ratios.

Fig. 5 shows model results for Standard and Fast SCR onset transients at various r-ratios, and demonstrates how indeed CI becomes more distinct with increasing r-ratio, or as the imbalance in r_{RHC} and r_{OHC} increases. As the CI becomes more distinct, the peak height grows, and the tail becomes faster or temporally shorter. For these results, the OHC rate coefficient (k_{OHC}) was specified to achieve a desired SS conversion, and k_{RHC} was determined from the k -ratio ($k_{\text{RHC}}/k_{\text{OHC}}$), at fixed k_{OHC} . The model predicts CI for other kinetic-parameter values beyond those used for the examples in **Fig. 5**. In general, increasing the k-ratio at a fixed k_{OHC} increases the magnitude and speed of the CI transient, as well as the SS $[\text{Cu}^{\text{I}}]$ and SS conversion. Based on these trends, anything that reduced r_{RHC} relative to r_{OHC} would be expected to reduce CI; this, in addition to the possibility of alternate reaction pathways, is consistent with CI being less apparent with Fast SCR relative to Standard SCR. **Figs. 4 and 5** imply that CI becomes increasingly apparent at higher temperature; consistent with our experimental observations that CI becomes increasingly apparent over Cu/SCR catalysts with increasing temperature for both Standard and Fast SCR (cf. **Fig. 1**).

Fig. 6 shows the impact of sweeping $[\text{NO}]$ at constant $[\text{NH}_3]$ on CI-parameter transients; the model results are consistent with the experimentally observed spatiotemporal CI trends, and indicate that CI is most apparent at higher absolute RHC and OHC rates. The N_2 and NO CI transients become progressively more distinct with increasing $[\text{NO}]$. These N_2 & NO CI transients balance (i.e., Eq. (5) stoichiometry), and the NO CI trends reflect those of **Fig. 2** where CI is more distinct in regions of high $[\text{NO}]$ towards the catalyst front. **Fig. 6c** shows corresponding r-ratio transients, and evidence that additional parameters beyond the r-ratio being greater than unity influence the CI nature. The r-ratio transient is progressively faster with increasing $[\text{NO}]$, although for all feed combinations the r-ratios converge to unity ($r_{\text{RHC}} = r_{\text{OHC,S}}$)

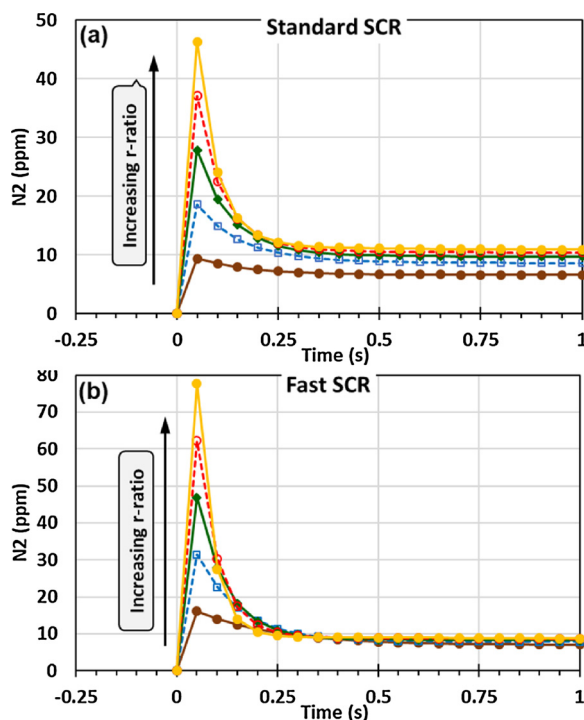


Fig. 5. Results from two-step (RHC & OHC) kinetic models of the Cu/SCR redox cycle showing CI variations with r-ratio for (a) Standard and (b) Fast SCR, with $\text{NO}_x:\text{NH}_3 = 200:200$ ppm. (a) The Standard SCR model used $k_{\text{OHC},\text{S}} = 3\text{E-}6$, and r-ratios of 58, 115, 173, 230, and 288 (k-ratios of 2E4, 4E4, 6E4, 8E4, and 10E4). (b) The Fast SCR model used $k_{\text{OHC},\text{F}} = 5\text{E-}2$, and r-ratios of 23, 45, 68, 90, and 113 (k-ratios of 4, 8, 12, 16, and 20).

at SS. Notably, Fig. 6c shows how the least distinct CI case (Fig. 6a & b, 50 ppm NO) has greater r-ratio values throughout the CI transient than the most distinct CI case (Fig. 6a & b, 250 ppm NO). While these cases arrive at the same SS Cu^{II} -limited condition and Cu partitioning, the CI is more distinct when the transient is fast. Similarly, as the r-ratio transient slows, the CI slows and the peak becomes smaller, suggesting that practical signal-to-noise implications may limit the ability to measure the slowest and least distinct CI transients. Clearly, CI distinctiveness is related to the speed at which the half-cycle rates balance. Fig. 6d shows the r_{RHC} and $r_{\text{OHC},\text{S}}$ transients for the various feed cases, and further demonstration of how the half-cycle rates converge at SS; the log scale spatially distorts the patterns, but it is clear from the absolute values that most of this rate convergence is attributable to r_{RHC} slowing. With increasing [NO], both initial RHC and OHC rates increase, the SS balanced half-cycle rate increases, and the transient becomes faster. While both r_{RHC} and $r_{\text{OHC},\text{S}}$ are first order in [NO] (cf. Eqs. (2) & (4)), and fixed [NO] steps will proportionally increase each rate, the absolute impact of a given [NO] step is greater on r_{RHC} . The salient point is that with increasing [NO], the imbalance between the RHC and OHC rates becomes more apparent, the RHC and OHC rate transients occur faster, and the SS Cu^{II} -limited state is reached faster; all of these characteristics contribute to more distinct CI. Thus, while the r-ratio is independent of [NO], as apparent from the ratio of Eqs. (2) & (4), the [NO] nevertheless impacts the CI nature via its influence on the absolute RHC and OHC rates, and corresponding speed of the rate transients. In summary, CI occurs for r-ratios greater than unity and is more distinct at higher initial RHC and OHC rates, which correspond to higher [NO]. These considerations are consistent with CI being greatest at the catalyst front where [NO] is higher, and progressively degrading along the catalyst axis with increasing NO conversion, as observed experimentally (cf. Fig. 2).

The model formulation reflects the predicted CI nature, and the consistency of those predictions with experiments validate the

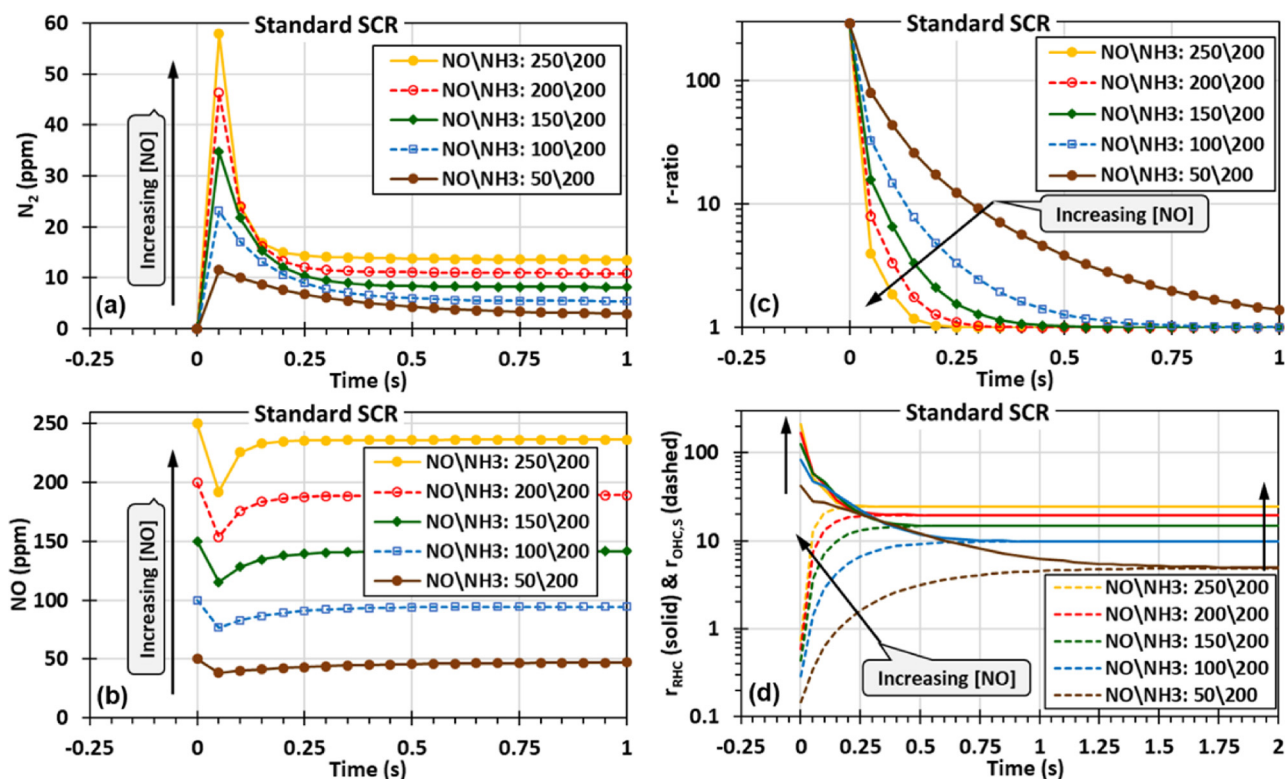


Fig. 6. Standard-SCR-onset CI transient parameters for sweeping NO (50, 100, 150, 200, 250 ppm) at constant NH_3 (200 ppm). (a) N_2 CI, (b) NO CI, (c) r-ratio, and (d) r_{RHC} (solid lines) and $r_{\text{OHC},\text{S}}$ (dashed lines) transients with a fixed $k_{\text{OHC},\text{S}}$ (3E-6) and k-ratio (1E5). The same rate-transient trends shown here for increasing [NO] will also occur at fixed feed concentration and increasing r-ratio.

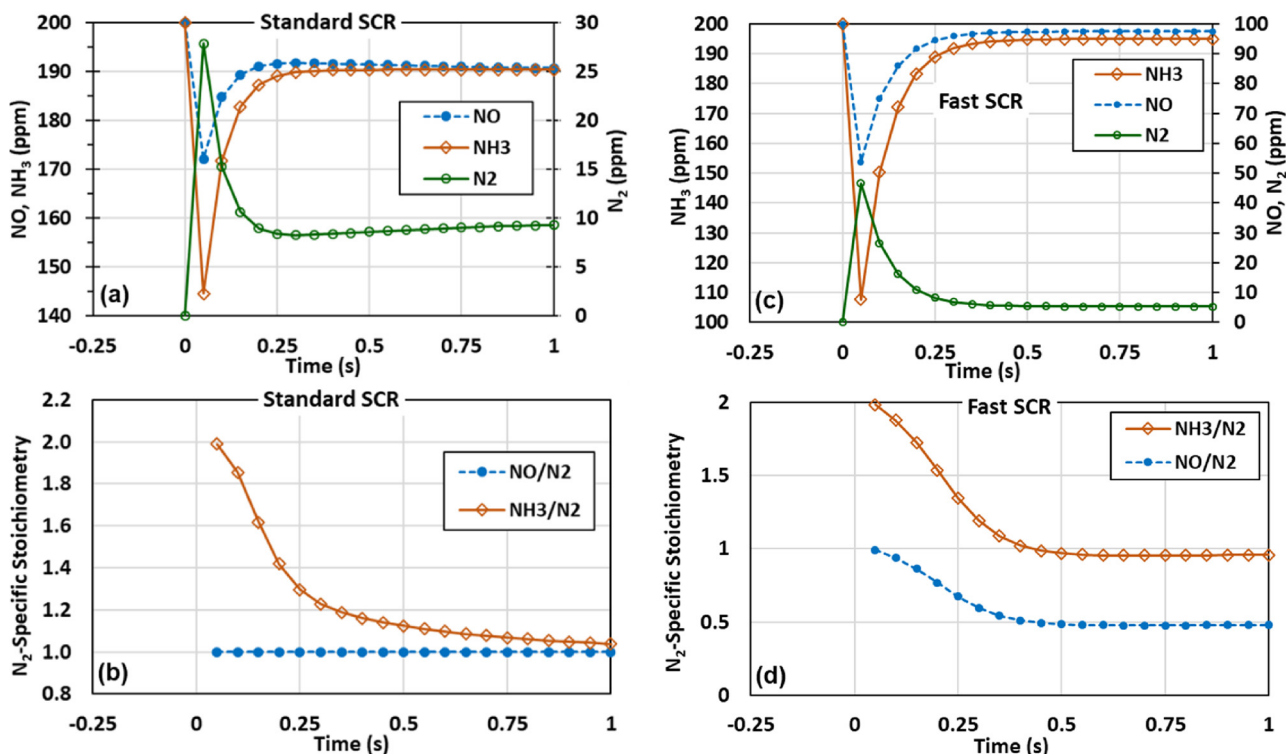


Fig. 7. SCR-onset transients for Standard (a & b) and Fast (c & d) SCR, showing NO, NH₃ and N₂ CI (a & c) and the corresponding stoichiometry transient (b & d). Standard SCR, NO\NH₃: 200\200 ppm, $k_{OHC,S} = 3E-6$, and k-ratio = 6E4. Fast SCR, NO\NO₂\NH₃: 100\100\200 ppm, $k_{OHC,F} = 3E-2$, and k-ratio = 20.

formulation. The result of Fig. 6 can be compared to similar results from sweeping [NH₃] at constant [NO], and sweeping [NO] and [NH₃] together; results shown in Appendix B. Not surprisingly, with the r_{RHC} zeroth order in θ_{NH_3} , the various CI and r-ratio transients are invariant for sweeping [NH₃] at constant [NO], and identical to Fig. 6a & c for sweeping [NO] and [NH₃] together. For different model formulations, the results would vary accordingly. For the model presented here, the influence of ANR variations on CI depends on if those variations are driven by NO or NH₃ changes. The ratio of Eqs. (2) & (4) shows that the r-ratio is independent of [NO], [NH₃] and ANR. However, as discussed above, NO influences CI nature via its impact on the r_{RHC} and r_{OHC} absolute initial magnitude and transient balancing speed, and thus NO-induced ANR changes will produce CI variations. In contrast, with the rates zeroth order in θ_{NH_3} , NH₃ variations will produce neither variations in the r-ratio or speed of the rate transients, and thus CI will be invariant with NH₃-induced ANR changes.

SCR-onset CI transients will produce corresponding stoichiometry transients reflecting the model formulation, and can be compared to measurements for validation. Fig. 7a & c show NO, NH₃ and N₂ CI model results for Standard and Fast SCR, respectively; the corresponding N₂-specific NO and NH₃ stoichiometry transients are shown in Fig. 7b & c, respectively. The initial values of NH₃/N₂ = 2, and NO/N₂ = 1 for both Standard and Fast SCR are consistent with Eq. (1) and the RHC dominating initial CI onset. Similarly, the SS stoichiometry ratios are consistent with the overall reaction stoichiometry for both Standard and Fast SCR (cf. Eqs. (5) & (8)); NH₃/N₂ = NO/N₂ = 1 for Standard SCR, and NH₃/N₂ = 1 and NO/N₂ = 0.5 for Fast SCR. Between these end points, a continuous stoichiometry transient occurs reflecting the progressive decreasing dominance of the RHC, and balancing of the RHC and OHC rates at SS. In general, the RHC dominates at CI onset, and the influence of the two half cycles become equivalent at SS. As such, the end points, possibly extrapolated in actual measurement data, can be used as further validation of model structure. For instance, beyond the comparison of Fig. 7b & c with Eqs. (1), (5) & (8), the Standard-SCR NO/N₂ would not be invariant and unity through the

CI transient without incorporating NO in the OHC. The polar nature of species like NH₃ and NO₂ cause instrument-surface interactions which lower the transient response of SpaciMS for such species [18,19], and thus the predicted NH₃ CI will not be measured by SpaciMS as configured; with improved instrument response, the predicted NH₃ CI may be measured. Nevertheless, the high temporal resolution of SpaciMS for practically nonpolar species like N₂ and NO allows the corresponding CI and related stoichiometry transient to be measured.

These examples highlight how reaction formulation and kinetic parameters influence the CI nature, and how CI analysis can be used to elucidate the same. The influence of numerous parameters on measurable CI characteristics, which can be used for guiding and validating half-cycle-based SCR models, has been shown; these include impacts of temperature, feed composition and concentrations, k_{OHC} , and r-ratio. The model results are consistent with many experimental observations regarding CI nature. Figs. 4 and 5 imply that CI becomes increasingly apparent at higher temperature; consistent with our experimental observations that CI becomes increasingly apparent over Cu/SCR catalysts with increasing temperature for both Standard and Fast SCR (cf. Fig. 1). Moreover, the model formulation is consistent with the experimentally observed spatial trends of greater r_{RHC} , and thus more distinct CI, at the catalyst front where NO is greatest (see Fig. 2), and that Fast SCR may mitigate CI by increasing $r_{OHC,F}$ and correspondingly reducing the r-ratio. Beyond the logic-based discussions related to Fig. 3, the model results quantitatively demonstrate how half-cycle rate imbalances produce CI, and demonstrate the ability to model CI via the two half cycles. It also shows how the detailed CI shape and nature are related to the various kinetic parameters; e.g., the pre-exponential factor influences the CI-onset temperature (r-ratio = unity), k_{OHC} largely impacts the SS conversion, and the feed concentrations, r-ratio, and absolute rates control the CI shape. This is the first redox-cycle model describing Cu/SCR CI, and provides a basis for experimentally determining kinetic parameters of the individual half cycles.

Table 1

Five-step protocol used to evaluate onset-transients of individual and combined redox-cycle components.

Step	Name	Composition
1.	Base	5% H ₂ O + 200 ppm NO _x in Ar
2.	RHC	Base + 200 ppm NH ₃
3.	OHC	Base + 0.4% O ₂
4.	SCR	Base + 0.4% O ₂ + 200 ppm NH ₃
5.	OHCb	Base + 0.4% O ₂

4. Experimental characterization of onset transients for Cu/SCR redox-cycle components

A commercial 400cpsi honeycomb-monolith Cu/CHA SCR catalyst was used for the experimental studies. The catalyst was field aged by an industrial user under actual commercial driving conditions. A 21-cell catalyst core (0.7-cm wide, 2.53-cm long) was prepared and evaluated at various temperatures (210, 300, 400, 500 & 600°C) and 40k/hr SV, using a bench reactor described previously [1]. Spatiotemporally resolved intra-catalyst measurements were implemented via custom direct-sampling SpaciMS (200 μm OD capillaries with ca. 10 μL/min sampling rate) [1,16–19].

Experiments were performed to probe onset transients associated with the individual and combined SCR-redox half cycles via a 5-step protocol implemented with Standard-, NO₂- and Fast-SCR mixtures described in Table 1 and Fig. 8. At the Base-to-RHC (Step1-2) transition, NH₃ is switched on, activating the RHC and populating Cu¹; the lack of an oxidizer (under Standard SCR) prevents Cu reoxidation, and at SS, this should produce the maximum Cu¹ concentration. Clearly there should be an RHC-onset CI associated with initially rapid and subsequently slowing RHC as the Cu^{II} population is depleted. At the RHC-to-OHC (Step 2–3) transition, NH₃ is switched off and O₂ is switched on activating OHC, and returning the Cu partitioning to the base Cu^{II}-biased state; OHC-onset CI transients can be observed as the Cu¹ population is depleted, slowing the OHC rate. The SCR-onset (Step 3–4) transient is studied by adding NH₃ to the OHC conditions; in this SCR condition, both RHC and OHC are simultaneously active, and thus the SS Cu¹ population should be less than that under the SS RHC condition. The SCR-to-OHCb (Step 4–5) transient involves switching NH₃ off, and is identical to the OHC transient except that it starts from a lower Cu¹ concentration; in cases where this transition starts from an OHC-limited condition (i.e., when there is a CI at SCR onset) an OHCb-onset CI will not occur. Thus, while CI can occur at OHC onset, it will not at OHCb

onset as confirmed by the experimental results (see Fig. 8). The detailed nature of the various onset transients provides insights regarding the SCR process, and rich data for determining kinetic parameters of the individual half cycles.

4.1. Experimental results and discussion

Fig. 9a shows the RHC-onset N₂ transient for the three SCR mixtures at 1/8 L from the catalyst front (L: catalyst length); OHC is not intentionally activated as O₂ is absent from the feed gas. The Standard-SCR onset transient shows CI indicating $r_{RHC} > r_{OHC,S}$, with a fast step-like leading edge indicative of the native RHC rate. The RHC rate slows over ca. 200 s as Cu^{II} is practically depleted; in this state the Cu^{II} population does not go to zero, although the Cu-inventory becomes significantly Cu¹ biased [4]. The small (~4.5 ppm N₂) SS conversion, indicates a small non-zero OHC, and could be due to feed gas oxidizer contaminant (e.g., O₂ or NO₂), or bulk lattice oxygen. Practically identical step-like RHC-onset transients are apparent for the NO₂- and Fast-SCR mixtures. Assuming the redox model, the absence of CI indicates that OHC is active and faster than or as fast as RHC for these cases. Moreover, the OHC and OHCb onset transients are practically equivalent for NO₂ and Fast SCR (Fig. 9b & d), other than the initial high-frequency dynamic with OHCb as discussed below; this similarity suggests that $r_{OHC,F}$ is practically identical for NO₂ and Fast SCR.

Fig. 9c shows protocol SCR-onset transients where O₂ is included in the gas feed and both half cycles are intentionally active. The Standard-SCR-onset CI indicates that RHC is initially faster than OHC, and then slows to match OHC at SS; with active OHC, the transient approach to SS is much faster (ca. 100 s) compared to the RHC case (ca. 200 s). The fast step-like onset transient is identical to the RHC-onset. Greater SS conversion occurs due to the presence of feed gas O₂ activating the OHC. Fast and NO₂ SCR display step-like onset transients without CI, indicating that OHC is not limiting SCR as in the Standard-SCR case. Notably, the fast onset transient and SS conversion are practically identical to that for RHC onset (Fig. 9a), suggesting that NO₂ is the main OHC driver (Cu^{II} repopulation), and that in this case O₂ is not practically contributing; consistent with being the higher-probability OHC activator [12]. While Cu-partitioning dynamics associated with the individual half cycle transients have been resolved with lower temporal resolution (192 s data increments) [13], these are the first measurements to resolve that dynamic balancing at SCR onset; and with much greater temporal resolution (0.7 s data increments).

Figs. 9b and d show the measured OHC- & OHCb-onset transients for the three SCR mixtures. For each case, the onset transients for Fast and

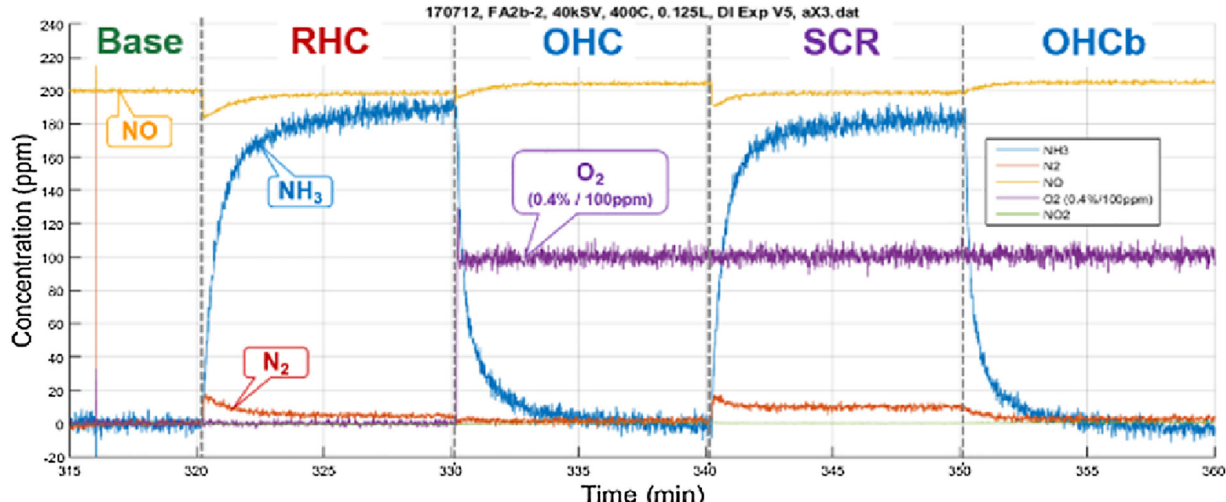


Fig. 8. Species concentrations, at 400°C, over the Standard-SCR 5-step protocol investigating onset transients associated with the individual and combined SCR-redox half cycles.

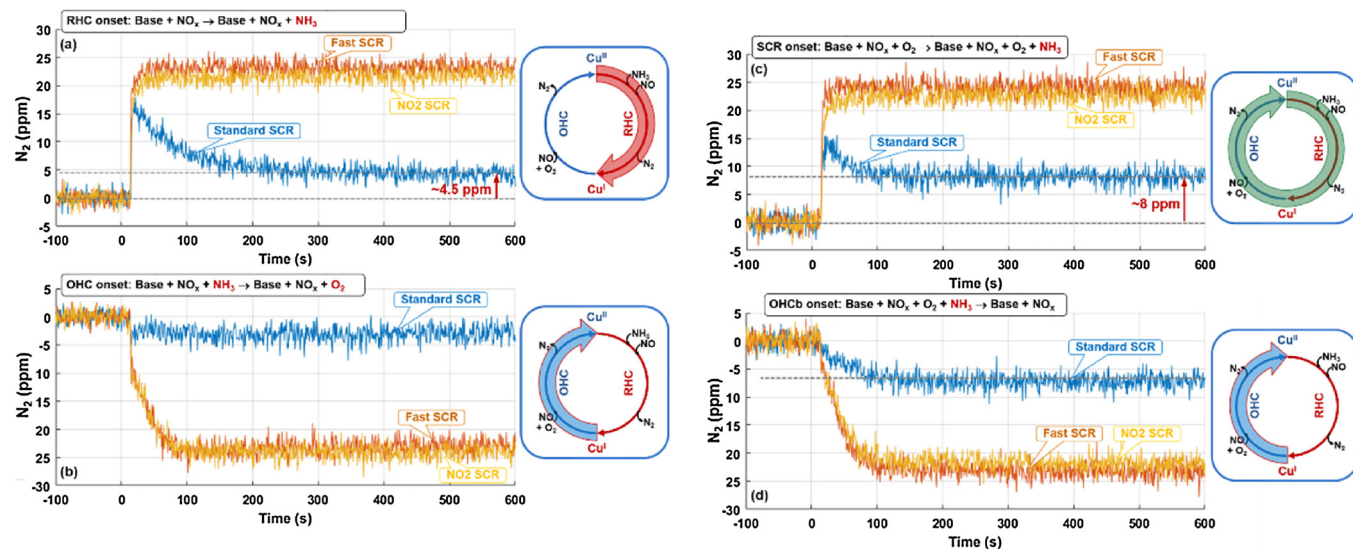


Fig. 9. Relative N_2 Onset transients at 400°C for the 5-Step Protocol steps with Standard-, NO_2 - & Fast-SCR mixtures. (a) RHC, (b) OHC, (c) SCR, (d) OHCb. Transients are relative to the N_2 baseline prior to the transition; thus, the OHC transients (b & d) have negative relative values.

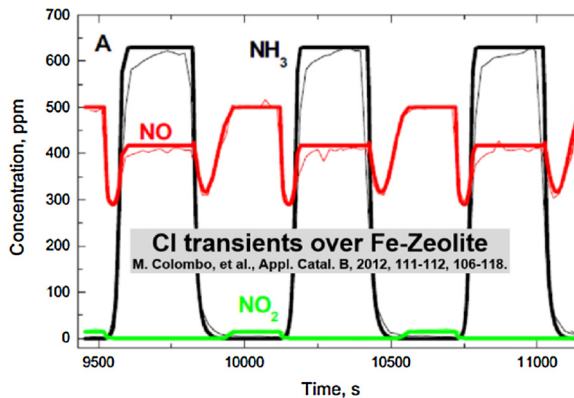


Fig. A1. CI in the effluent of an Fe/SCR catalyst due to transient NH_3 -coverage buildup and depletion through a threshold level corresponding to the onset of NH_3 inhibition at SCR onset and termination [3]. At SCR onset starting from an NH_3 -free surface, conversion initially increases in a rapid step-like fashion with corresponding NH_3 -coverage buildup; such fast coverage buildup is consistent with it being a nonactivated process. Conversion slows with the initial onset of NH_3 inhibition, and can degrade with further coverage buildup well beyond that necessary for inhibition onset; the results is a transient CI, where the degree of inflection is proportional to the ratio of the saturated NH_3 capacity to that necessary for inhibition onset (greater inflection with greater ratio). In this example, the steady state conversion is ca. 50% that at the CI peak; i.e., double conversion could be achieved if NH_3 -coverage buildup could be halted at the CI peak. An SCR-termination CI will similarly occur starting from SCR in an inhibited state; i.e., conversion will increase as NH_3 coverage is consumed mitigating corresponding inhibition, but with increasing time, a subsequent inflection will occur as coverage is depleted and conversion correspondingly goes to zero. Thus, inhibition-driven CI occurs at both SCR onset and termination. Moreover, inhibition-induced CI should be more pronounced at conditions with higher NH_3 capacity; i.e., should be more pronounced at lower temperature, and less pronounced at higher temperatures where NH_3 capacity is lower.

NO_2 SCR are identical and occur over ca. $< 100\text{s}$. Because OHC-onset starts from a greater Cu^{I} concentration, it has a greater high-frequency initial onset component relative to OHCb; i.e., the initial step-like transient observed with OHC. While the signal-to-noise ratio is too small to well characterize the OSC-onset N_2 transient under Standard SCR conditions, onset CI was apparent in the NO transient for this same condition (see Fig. 8). For OHCb Standard SCR, a progressive ca. 150s -long response without CI is apparent from both the N_2 and NO data (see Fig. 8). This slower onset transient for Standard SCR relative to the Fast- and NO_2 -SCR cases is consistent with differing OHC mechanisms and kinetics for O_2 - and NO_2 -driven OHC [12].

5. Conclusions

The modeling and analytical techniques demonstrate several new capabilities for advancing NH_3 -SCR catalysis. The model shows how the SCR redox cycle can be modeled by two-step kinetics, and provides the

first demonstration of SCR-onset CI due to redox half-cycle rate imbalances. The step-response CI methodology provides a practical and broadly applicable technique for studying the redox cycle and dynamic Cu partitioning that can augment traditional XAS approaches [4,12,13]; i.e., improved temporal resolution, spatial resolution, can be applied to monolith-supported washcoat catalysts, and using more common laboratory equipment broadly accessible to the research community and applicable to a range of conditions and catalyst samples. Its application here provided the first measurements to resolve dynamic RHC-OHC rate (and Cu-partition) balancing at SCR onset.

The modeling and experiments demonstrate how SCR-onset CI transients are due to imbalances in the Cu-redox half-cycle rates, and specifically occur when RHC is initially faster than OHC. These have been used to probe the transient conversion nature associated with activating individual and combined half-cycles. In general, the model shows that CI becomes more distinct with increasing r-ratio and $[\text{NO}]$; this is consistent with our experimental observations of CI being more

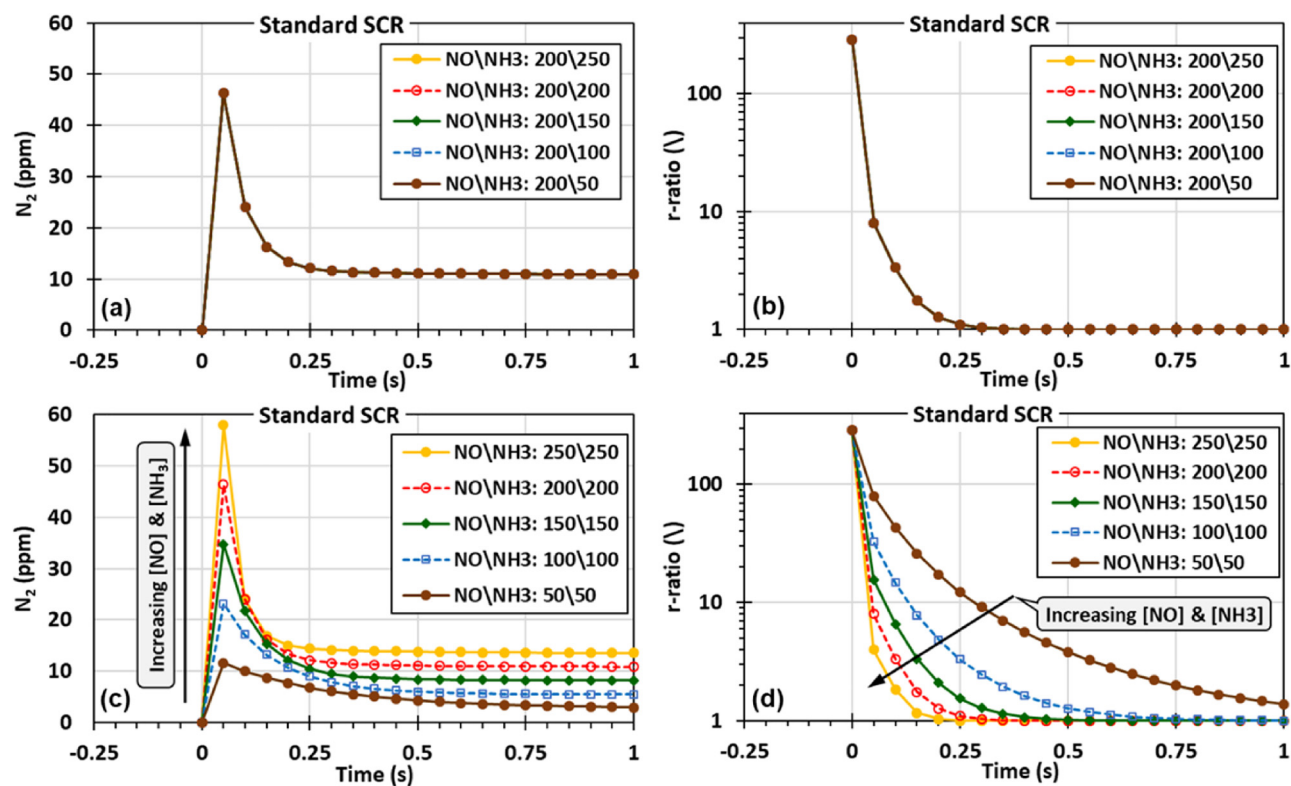


Fig. B1. SCR-onset N₂ CI transients (a & c) and corresponding r-ratio transients (b & d) for cases of sweeping NH₃ at constant NO (a & b) and sweeping NO and NH₃ together (c & d). For both cases $k_{OHC,S}$ (3E-6) and k -ratio (1E-5).

distinct at higher temperatures, at the catalyst front where [NO] is highest, and degrading along the catalyst axis as conversion progresses. Moreover, enhancing OHC rate will mitigate CI; e.g., as does NO₂ in Fast- and NO₂-SCR mixtures. Thus, Fast-SCR-onset CI being observed only at the highest temperatures investigated, indicating greater r_{RHC} temperature sensitivity than $r_{OHC,S}$. The detailed CI nature reflects the underlying kinetic parameters of the half cycles, and a wide range of CI transients can be probed under different conditions (RHC, OHC, SCR, OHCb), and over a range of temperatures. Modeling examples highlight how reaction formulation and kinetic parameters influence the CI nature, and how CI analysis can be used to elucidate the same. The influence of numerous parameters on measurable CI characteristics, including temperature, feed composition and concentrations, k_{OHC} , and r-ratio were shown; these can be used for guiding and validating half-cycle-based SCR models. This provides the basis of a step-response method for determining kinetic parameters of the individual Cu-redox half cycles using the CI transient measurements and a two-step model. In future work we will apply the methodology for that purpose.

Appendix A. NH₃-Coverage-Induced CI in Fe/SCR Catalysts

See Fig. A1.

Appendix B. Sweeping NH₃ at constant NO = 200 ppm, and sweeping NO & NH₃ together

See Fig. B1.

References

- [1] X. Auvray, W.P. Partridge, J.-S. Choi, J.A. Pihl, A. Yezerski, K. Kamasamudram, N.W. Currier, L. Olsson, Local ammonia storage and ammonia inhibition in a monolithic copper-beta zeolite SCR catalyst, *Appl. Catal. B* 126 (2012) 144–152.
- [2] W.P. Partridge, M.-Y. Kim, J.A. Pihl, C.S. Daw, J.-S. Choi, N. Currier, A. Yezerski, K. Kamasamudram, S. Joshi, Field-ageing impacts on a commercial automotive Cu/CHA SCR catalyst: focusing on NH₃ capacity utilization, DOE Crosscut Workshop on Lean Emissions Reduction Simulation, (2015) <http://cleers.org/workshops/workshop2015/index.php?presentation=1>.
- [3] M. Colombo, I. Nova, E. Tronconi, V. Schmeißer, B. Bandl-Konrad, L. Zimmermann, NO/NO₂/N₂O-NH₃ SCR reactions over a commercial Fe-zeolite catalyst for diesel exhaust aftertreatment: intrinsic kinetics and monolith converter modelling, *Appl. Catal. B* 111–112 (2012) 106–118.
- [4] C. Paolucci, A.A. Verma, S.A. Bates, V.F. Kispersky, J.T. Miller, R. Gounder,

W.N. Delgass, F.H. Ribeiro, W.F. Schneider, Isolation of the copper redox steps in the standard selective catalytic reduction on Cu-SSZ-13, *Angew. Chem. Int. Ed.* 53 (2014) 11828–11833.

[5] F. Gao, J.H. Kwak, J. Szanyi, C.H.F. Peden, Current understanding of Cu-exchanged chabazite molecular sieves for use as commercial diesel engine DeNO_x catalysts, *Top. Catal.* 56 (2013) 1441–1459.

[6] T. Yu, T. Hao, D. Fan, J. Wang, M. Shen, W. Li, Recent NH₃-SCR mechanism research over Cu/SAPO-34 catalyst, *J. Phys. Chem. C* 118 (2014) 6565–6575.

[7] J.-H. Kwak, J.H. Lee, S.D. Burton, A.S. Lipton, C.H.F. Peden, J. Szanyi, A common intermediate for N₂ formation in enzymes and zeolites: side-on Cu-nitrosyl complexes, *Angew. Chem.* 125 (2013) 9985–9989.

[8] T.V.W. Janssens, H. Falsig, L.F. Lundsgaard, P.N.R. Vennestrom, S.B. Rasmussen, P. Georg Moses, F. Giordanino, E. Borfecchia, K.A. Lomachenko, C. Lamberti, S. Bordiga, A. Godiksen, S. Mossin, P. Beato, A consistent reaction scheme for the selective catalytic reduction of nitrogen oxides with ammonia, *ACS Catal.* 5 (2015) 2832–2845.

[9] M.P. Ruggeri, I. Nova, E. Tronconi, J.A. Pihl, T.J. Toops, W.P. Partridge, In-situ DRIFTS measurements for the mechanistic study of NO oxidation over a commercial Cu-CHA catalyst, *Appl. Catal. B* 166 (2015) 181–192.

[10] T. Gunter, H.W.P. Carvalho, D.E. Doronkin, T. Sheppard, P. Glatzel, A.J. Atkins, J. Rudolph, C.R. Jacob, M. Casapu, J.-D. Grunwaldt, Structural snapshots of the SCR reaction mechanism on Cu-SSZ-13, *Chem. Comm.* 51 (2015) 9227–9230.

[11] C. Paolucci, A.A. Parekh, I. Khurana, J.R. Di Iorio, H. Li, J.D. Albarracin Caballero, A.J. Shih, T. Anggara, W.N. Delgass, J.T. Miller, F.H. Ribeiro, R. Gounder, W.F. Schneider, Catalysis in a cage: condition-dependent speciation and dynamics of exchanged Cu cations in SSZ-13 zeolites, *J. Am. Chem. Soc.* 138 (2016) 6028–6048.

[12] C. Paolucci, I. Khurana, A.A. Parekh, S. Li, A.J. Shih, H. Li, J.R. Di Iorio, J.D. Albarracin-Caballero, A. Yezerski, J.T. Miller, W.N. Delgass, F.H. Ribeiro, W.F. Schneider, R. Gounder, Dynamic multinuclear sites formed by mobilized copper ions in NO_x selective catalytic reduction, *Science* 357 (2017) 898–903.

[13] K. Ueda, J. Ohyama, A. Satsuma, In situ XAFS study of dynamic behavior of Cu species in MFI-Zeolite under element gases of ammonia selective catalytic reduction, *Chem. Lett.* 46 (2017) 1390–1392.

[14] M. Colombo, I. Nova, E. Tronconi, Detailed kinetic modeling of the NH₃-NO/NO₂ SCR reactions over a commercial Cu-zeolite catalyst for diesel exhausts after treatment, *Catal. Today* 197 (2012) 243–255.

[15] J.-Y. Luo, X. Hou, P. Wijayakoon, S.J. Schmieg, W. Li, W.S. Epling, Spatially resolving SCR reactions over a Fe/zeolite catalyst, *Appl. Catal. B* 102 (2011) 110–119.

[16] W.P. Partridge, J.M.E. Storey, S.A. Lewis, R.W. Smithwick, G.L. DeVault, M.J. Cunningham, N.W. Currier, T.M. Yonushonis, Time-resolved measurements of emission transients by mass spectrometry, *SAE Pap.* (2000) 01–2952.

[17] W.P. Partridge, J.-S. Choi, NH₃ formation and utilization in regeneration of Pt/Ba/Al₂O₃ NO_x storage-reduction catalyst with H₂, *Appl. Catal. B* 91 (2009) 144–151.

[18] K. Morgan, J. Touitou, J.-S. Choi, C. Coney, C. Hardacre, J.A. Pihl, C.E. Stere, M.-Y. Kim, C. Stewart, A. Goguet, W.P. Partridge, Evolution and enabling capabilities of spatially resolved techniques for the characterization of heterogeneously catalyzed reactions, *ACS Catal.* 6 (2016) 1356–1381.

[19] W.P. Partridge, J.-S. Choi, Understanding the performance of automotive catalysts via spatial resolution of reactions inside honeycomb monoliths, in: Olaf Deutschmann, Anthony G. Dixon (Eds.), *Spatially-resolved Operando Measurements in Heterogeneous Catalytic Reactors*, vol. 50, *Advances in Chemical Engineering Series*; Academic Press/Elsevier, Kidlington, United Kingdom, 2017 Chapter 1, 1–81, ISBN 978-0-12-812589-2.